Supporting Information

Facile one-step synthesis and enhanced photocatalytic activity of WC/ferroelectric nanocomposite

Man Zhang[a], Yaqiong Wang[b], Jianguo Liu[c], Madasamy Thangamuthu[d], Yajun Yue[e], Zhongna Yan[e,g], Jingyu Feng[f], Dou Zhang[g], Hongtao Zhang[h], Shaoliang Guan[i], Maria-Magdalena Titirici[f], Isaac Abrahams[e], Junwang Tang[d], Zhen Zhang[j], Steve Dunn[b]*, Haixue Yan[a]*

[a] School of Engineering and Materials Science, Queen Mary University of London, Mile End Road, London E1 4NS, UK

[b] School of Engineering, London South Bank University
103 Borough Road, London, SE1 0AA, UK

[c] School of Environment, Tsinghua University
1 Qinghuayuan, Beijing, 100084, China

[d] Department of Chemical Engineering, University College London, Torrington Place, London, WC1E 7JE, UK

[e] Department of Chemistry, Queen Mary University of London, Mile End Road, London E1 4NS, UK

[f] Department of Chemical Engineering, Imperial College London
South Kensington Campus, London SW7 2AZ, UK

[g] State Key Laboratory of Powder Metallurgy, Central South University
South Lushan Road, Changsha, 410083, China

[h] Department of Materials, Loughborough University
Leicestershire, LE11 3TU, UK

[i] School of Chemistry, Cardiff University
Main Building, Park Place, Cardiff, CF10 3AT

[j] Division of Solid State Electronics, Department of Electrical Science, Uppsala University
Lagerhyddsvagen 1, Uppsala, Sweden

Email : (H.Y. : h.x.yan@qmul.ac.uk)

(S. D. : dunns4@lsbu.ac.uk)

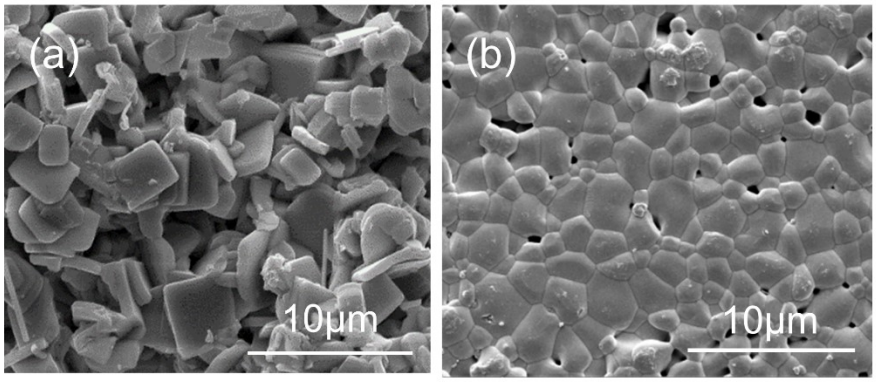

Fig. S1. SEM images of the natural surface of sintered ceramics: (a) $RbBi_2Ti_2NbO_{10}$, (b) $RbBi_2Nb_5O_{16}$

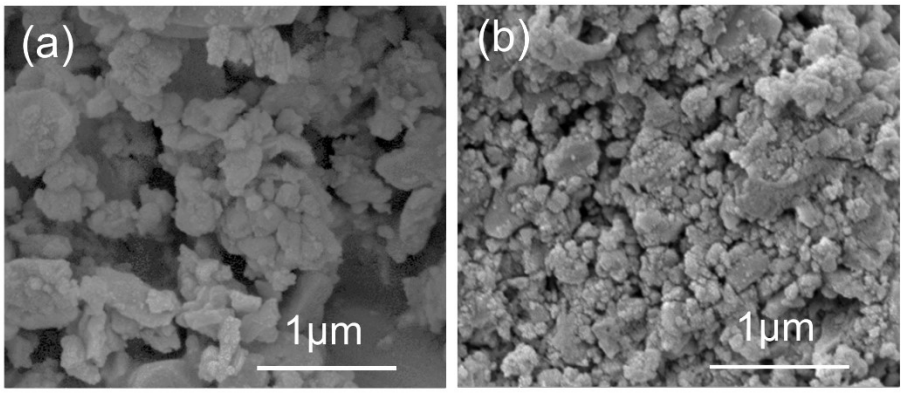

Fig. S2. SEM images of sub-micron sized powders used for photocatalytic property tests: (a) $RbBi_2Ti_2NbO_{10}$, (b) $RbBi_2Nb_5O_{16}$

Piezoresponse force microscopy (PFM) was used to confirm the ferroelectric nature of the sub-micron sized $RbBi_2Ti_2NbO_{10}$ powder. The average particle size of the sub-micron sized $RbBi_2Ti_2NbO_{10}$ powder was ~ 400 nm according to the SEM image shown in Fig. S2a. Vertical PFM scanning was performed on a chosen area of 1 × 1 μm. Fig S3 shows topography, amplitude and phase images of the powder. There is no change in topography with or without applied voltage. The magnitude of the amplitude image is proportional to the longitudinal piezoelectric constant (d_{33}) and the phase carries information on domain orientation (0 º when the field and polarization direction are parallel and 180 º when they are antiparallel). Fig. S3b-c depicts the PFM images of the initial $RbBi_2Ti_2NbO_{10}$ powder. When the sample is electrically poled by applying a + 10 V DC bias to the probe tip, obvious changes in the amplitude (Fig. S3e) and phase (Fig. S3f) images are observed compared with those in the virgin state (Fig. S3b, S3c), which indicate field induced ferroelectric domain switching. After applying a -12 V DC bias to the tip, the domains reverse switch, which is evidenced by the decreased contrast in Fig S3h and 3i. The switching of domains confirms the ferroelectric nature of sub-micron sized $RbBi_2Ti_2NbO_{10}$ powder.

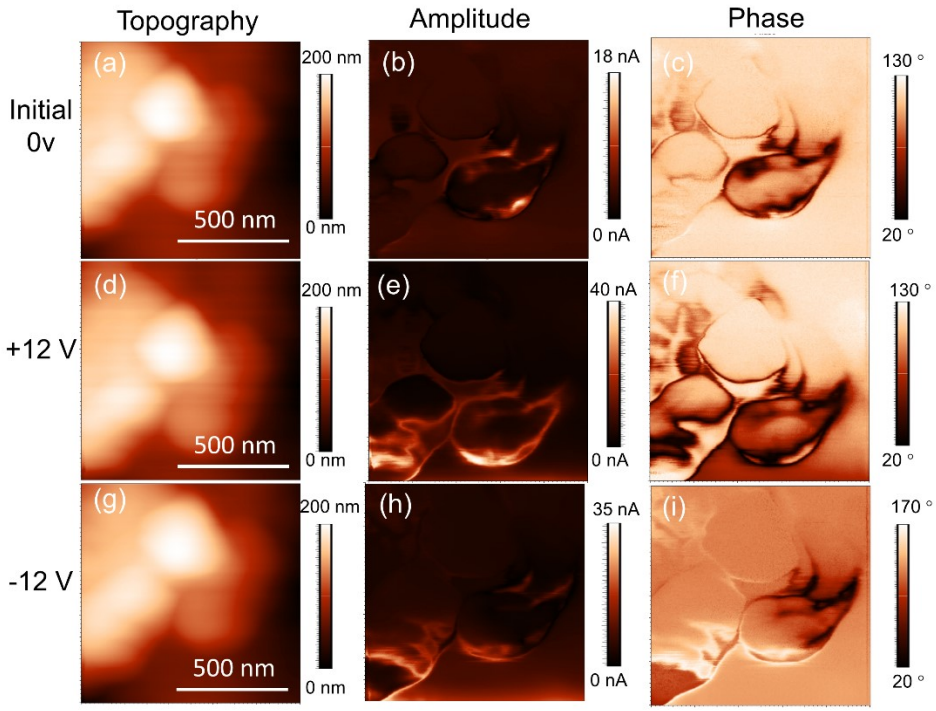

Fig. S3 PFM images of sub-micron sized $RbBi_2Ti_2NbO_{10}$ powder (obtained from a 1 × 1 μm^2 area on successive application of 0, + 12V and -12 V DC bias to the probe tip at room temperature); (a, d, g) topographical, (b, e, h) amplitude and (c, f, i) phase images.

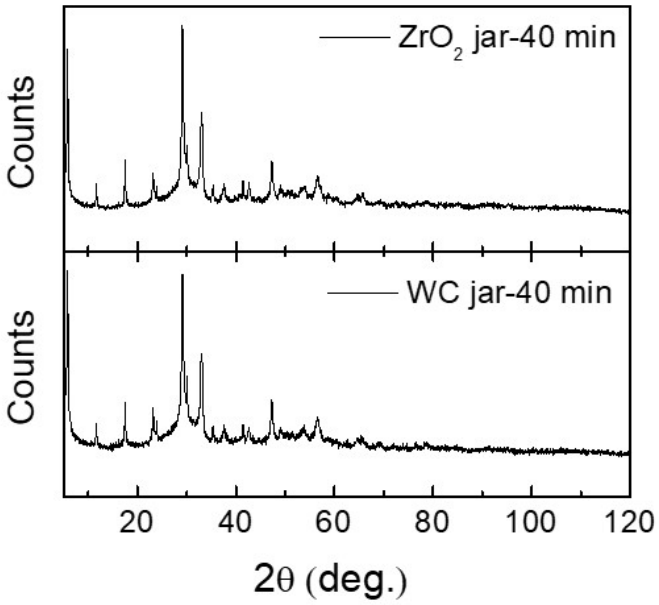

Fig. S4. XRD patterns of nano $RbBi_2Ti_2NbO_{10}$ powder ball milled in WC and ZrO_2 jars at a rotation speed of 600 rpm for 40 min.

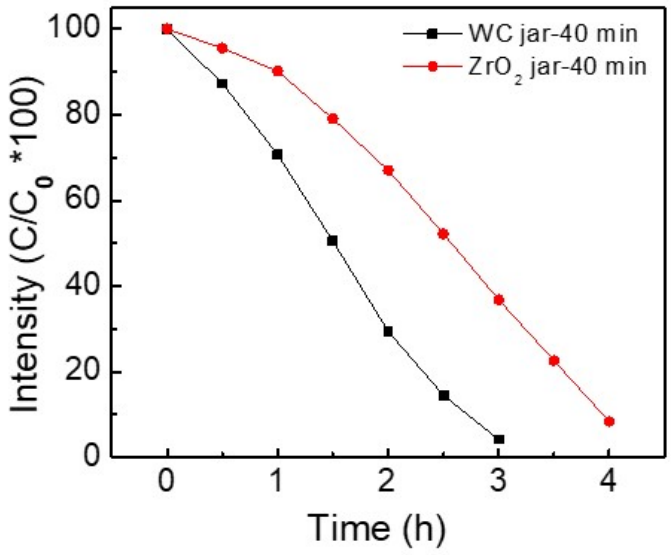

Fig. S5. Degradation of RhB using nano $RbBi_2Ti_2NbO_{10}$ powder ball milled in WC and ZrO_2 jars at a rotation speed of 600 rpm for 40 min.

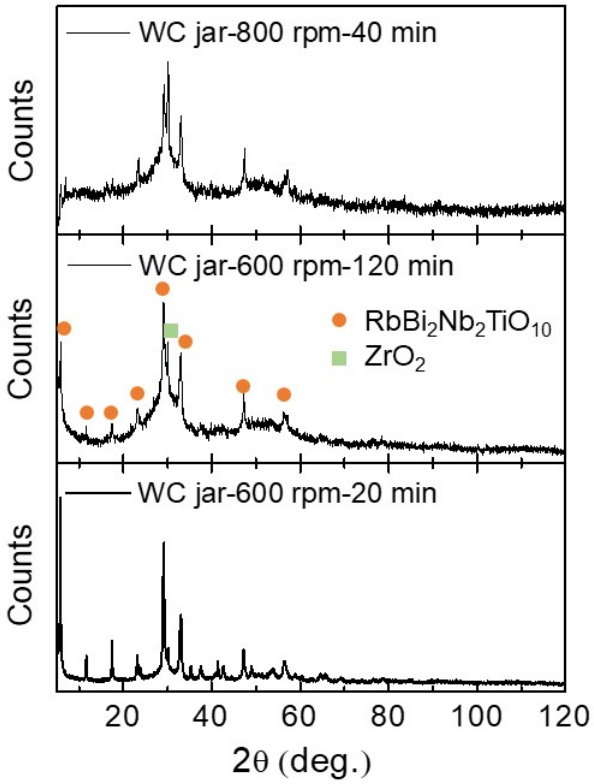

Fig. S6. XRD patterns of $RbBi_2Ti_2NbO_{10}$ nanocomposite ball milled in a WC jar under different conditions

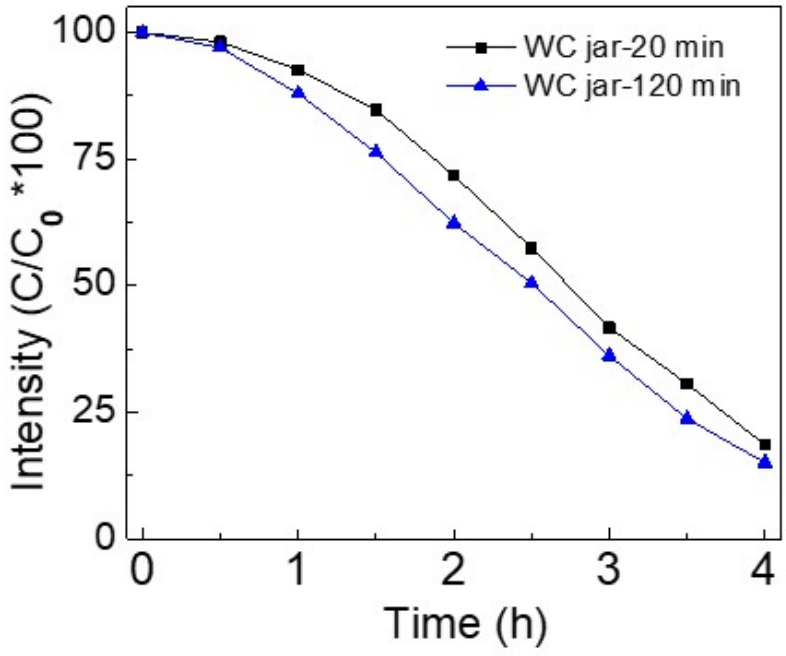

Fig. S7. Degradation of RhB using nano $RbBi_2Ti_2NbO_{10}$ powder ball milled in a WC jar for 20 min and 120 min at a rotation speed of 600 rpm.

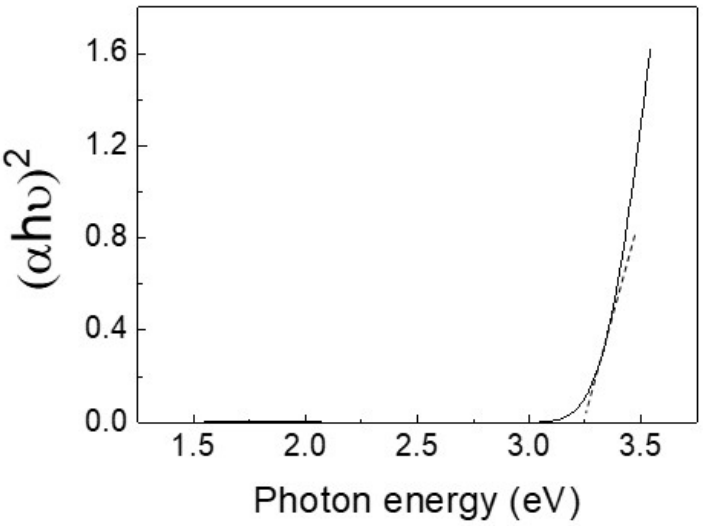

Fig. S8. Derived Tauc plot of WC/$RbBi_2Ti_2NbO_{10}$ nanocomposite, where the dashed line is the tangent of the linear part.

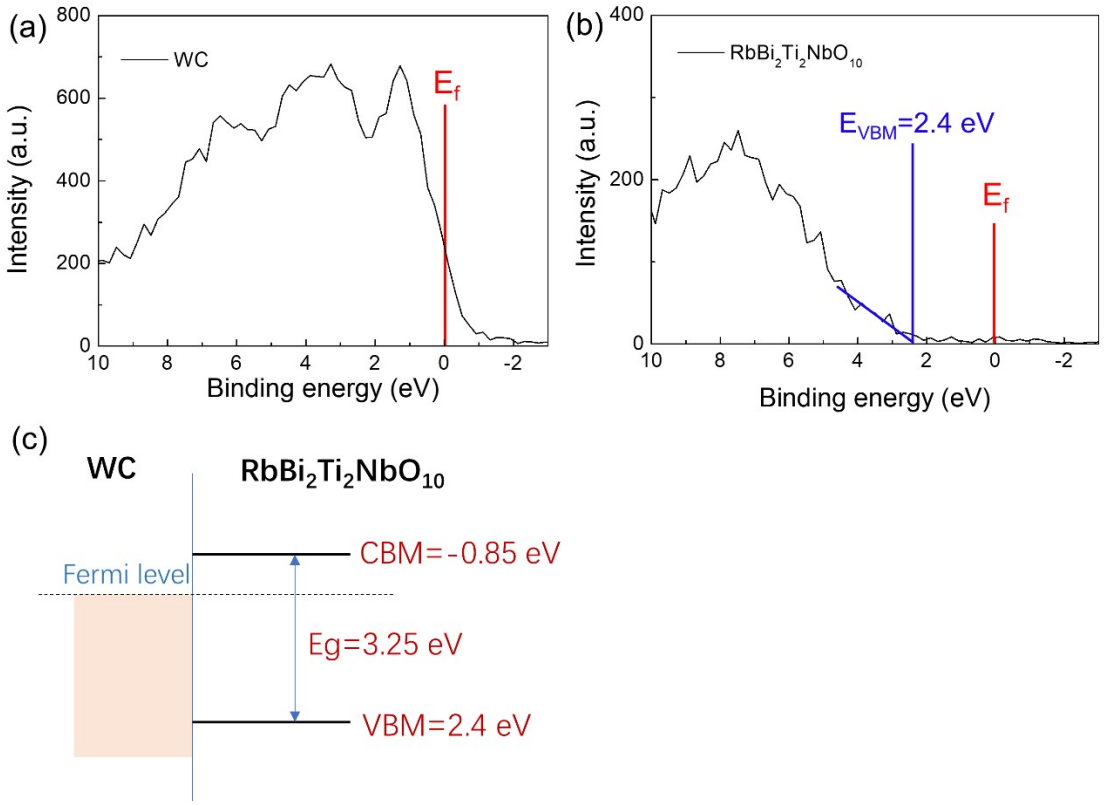

Fig. S9. X-Ray Photoelectron valence band spectra of (a) WC; (b) $RbBi_2Ti_2NbO_{10}$; (c) band structure of WC and $RbBi_2Ti_2NbO_{10}$. The Fermi level of WC is confirmed using the method given in reference [1].

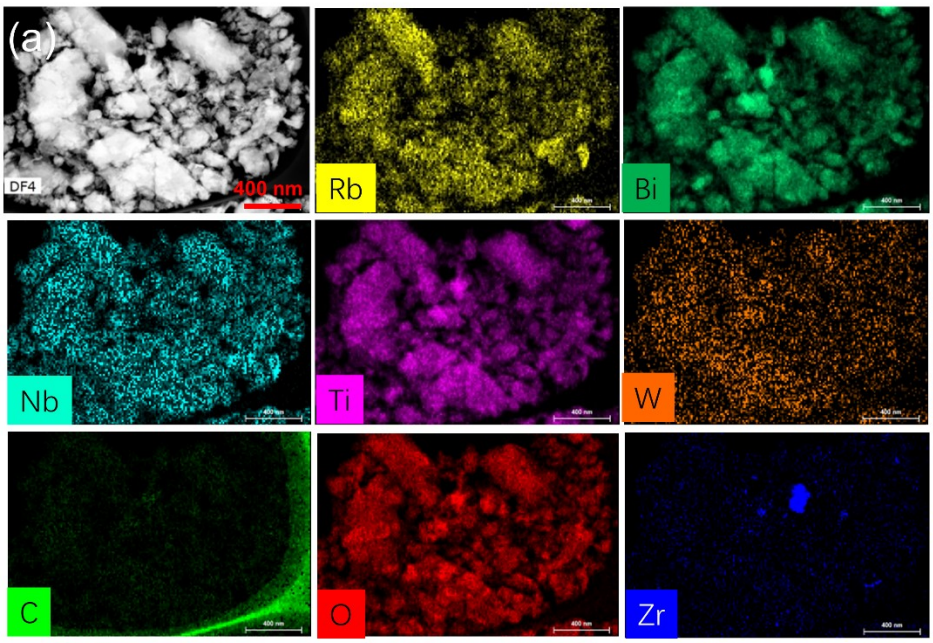

Fig. S10. TEM image and EDX elemental maps of WC/$RbBi_2Ti_2NbO_{10}$ nanocomposite.

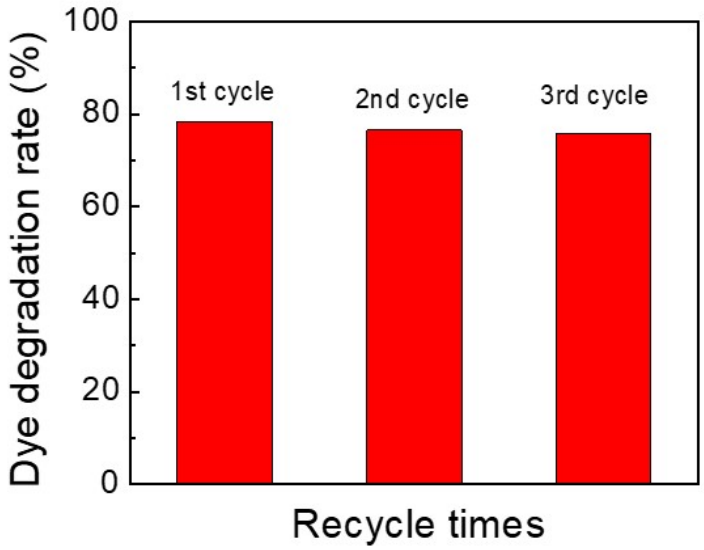

Fig. S11. Recyclability of WC/$RbBi_2Ti_2NbO_{10}$ nanocomposite. Each cycle lasted for 1.5 h.

Table S1. Photocatalytic properties of WC/ $RbBi_2Ti_2NbO_{10}$ nanocomposites ball milled under different rotation speeds for different durations

Jar type	Ball milling speed (rpm)	Ball milling time (min)	Specific surface area (m^2 g^{-1})	Degradation rate (min^{-1})
WC	600	20	15.87	0.007
WC	600	40	19.47	0.016
WC	600	120	25.02	0.007
WC	800	40	19.77	0.023

Reference

[1] L.H. Bennett, J.R. Cuthill, A.J. Mcalister, N.E. Erickson, R.E. Watson, Electronic structure and catalytic behavior of tungsten carbide, Science. 184 (1974) 563–565.